

Stability of short, single-mode erbium-doped fiber lasers

Mikael Svalgaard and Sarah L. Gilbert

We conducted a detailed study of the stability of short, erbium-doped fiber lasers fabricated with two UV-induced Bragg gratings written into the doped fiber. We find that the relative intensity noise of single-longitudinal-mode fiber grating lasers is approximately 3 orders of magnitude lower than that of a single-frequency 1.523- μm helium–neon laser. The frequency noise spectrum contains few resonances, none of which exceeds 0.6 kHz/Hz^{1/2} rms; the integrated rms frequency noise from 50 Hz to 63 kHz is 36 kHz. We also demonstrate a simple method for monitoring the laser power and number of oscillating modes during laser fabrication.

Key words: Fiber lasers, Bragg gratings, frequency stability, intensity noise, relaxation oscillations.

1. Introduction

Single-longitudinal-mode erbium-doped fiber lasers have recently received considerable attention as light sources for applications such as telecommunications,¹ sensors,² and metrology.^{3,4} Modern devices use UV-induced Bragg gratings written directly into the fiber for optical feedback and frequency selection, thereby avoiding mechanical instability associated with bulk components. Robust single-mode operation has been demonstrated with use of two gratings 1–2 cm apart.⁵

Our main focus in this paper is to investigate the frequency stability of Er-doped fiber lasers that incorporate Bragg fiber gratings as the end mirrors. Self-heterodyne measurements show that these lasers have linewidths of approximately 10 kHz. However, such measurements are insensitive to frequency jitter occurring at low frequencies, below approximately 10 kHz, which is the range where mechanical instabilities typically occur. Using a weakly locked, narrowband Fabry–Perot filter, we extended these investigations to include the intensity and frequency noise in the low-frequency regime from 50 Hz to 100 kHz. We find that short, single-mode Bragg-grating fiber lasers are substantially less susceptible to mechanical instabilities than their bulk

component counterparts. When not hampered by relaxation oscillations, the stability of such devices approaches the limit imposed by phase noise that is due to thermal fluctuations of the laser cavity.

Because typical Bragg gratings have bandwidths of a fraction of a nanometer, the operation of such a device will depend critically on how well the two gratings match each other in wavelength. This complicates the laser fabrication, since the dynamics of forming Bragg gratings involves spectral shifts of the same order of magnitude as the grating bandwidth. In this paper we show that such small changes during UV writing critically affect the performance of the resulting fiber laser. To deal with this problem we demonstrate a simple method for real-time monitoring of the laser performance based on simultaneous UV grating fabrication and pumping of the Er-doped fiber.

2. Experimental Setup

The UV production and grating apparatus are described in Ref. 6. Ultraviolet radiation is generated by frequency doubling an argon-ion laser operating at 488 nm with a beta barium borate (BBO) crystal in an external, actively stabilized ring cavity. We generate as high as 80 mW of continuous-wave 244-nm radiation with this setup. To fabricate Bragg gratings, a UV interference pattern is produced with a silica prism interferometer that is placed on top of a photosensitive Er-doped fiber. The angle of incidence on the prism determines the UV interference pattern periodicity Λ , and thus the Bragg wavelength $\lambda_B = 2n_{\text{eff}}\Lambda$, where n_{eff} is the guided mode effective index. For this study, the Bragg wavelength was set

When this research was undertaken both authors were at the National Institute of Standards and Technology, 325 Broadway, Boulder, Colorado 80303. M. Svalgaard is currently with the Microelectronics Center, Technical University of Denmark, Building 345 East, Lyngby DK-2800 Denmark.

Received 23 September 1996.

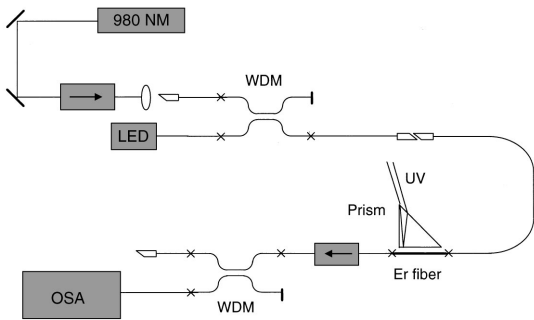


Fig. 1. Schematic drawing of the experimental setup used for fiber laser fabrication and real-time characterization.

near 1530 nm. The UV beam is focused onto the fiber with a cylindrical lens. The UV spot at the fiber forms a line along the fiber axis with a width (FWHM) of approximately 15 μm and a total length of approximately 3.5 mm.

When fabricating gratings for fiber lasers we splice both ends of a 10-cm Er-doped fiber to standard telecommunications fiber. To monitor the fiber laser performance, we can pump the Er-doped fiber and monitor the laser output on a spectrum analyzer during the grating inscription. In this way, we can, in real time, monitor both the output power and the number of longitudinal modes of the fiber laser as the second feedback grating is written.

The setup is shown in Fig. 1. The Er-doped fiber was pumped by a 980-nm, multimode diode laser through a 1530–980-nm wavelength division multiplexing (WDM) fiber coupler. For characterization, light from a broadband 1550-nm light-emitting diode (LED) (or a white-light source) could be launched into the fiber through the other arm of this WDM fiber coupler. After the Er-doped fiber, another WDM fiber coupler separated the laser and pump signals. To prevent feedback we used optical isolators after both the diode and the fiber lasers, and all fiber ends were angled. The fiber laser output could be monitored on either a 0.05-nm resolution optical spectrum analyzer (OSA) or a scanning Fabry–Perot interferometer (1.5-GHz free spectral range, finesse ≈ 170).

Using the broadband sources, we measured the absorption of the Er-doped fiber to be 13 dB/m at 980 nm and 18 dB/m at 1530 nm.⁷ We measured the small signal gain using the LED as a probe signal and simultaneously pumping the Er-doped fiber in the 980-nm band. We measured the saturated small signal gain to be 17 dB/m at 1529 nm. This is an indication that gain-reducing dissipative processes such as ion-ion interactions are small in this fiber. The fiber was sufficiently photosensitive that we did not need to use photosensitization techniques such as H_2 loading.

3. Laser Fabrication

The grating formation dynamics were monitored in transmission with the LED source. For all fiber lasers discussed in this paper the first grating was

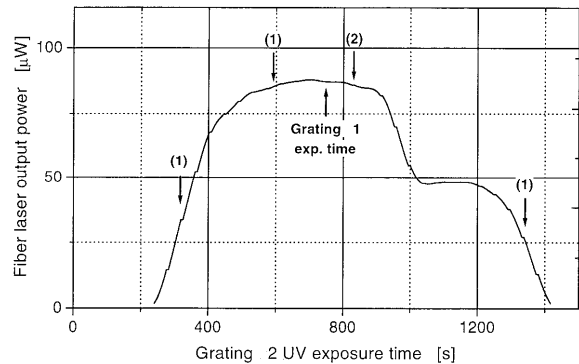


Fig. 2. Fiber laser output versus the second grating (grating 2) UV exposure time. The exposure time of the first grating (grating 1) is indicated by an upward pointing arrow. The downward pointing arrows correspond approximately to fiber lasers that were sampled for further investigation. The number of longitudinal modes present is indicated by numbers above the arrows. The pump power is approximately 50 mW.

exposed until the transmittance at the Bragg wavelength was 0.028 ± 0.001 . During this time the Bragg wavelength had shifted approximately 0.3 nm, which corresponds to an effective index change of approximately 3×10^{-4} . For longer exposure times the reflectance began to decline, possibly due to imperfect visibility or instability of the UV interference pattern. The spectral bandwidth of the gratings was rather broad, typically 0.6–0.8 nm FWHM, mainly due to the magnitude of the index change required to produce high reflectance with the relatively short gratings.

To obtain robust single-frequency operation, the cavity must be short. After writing the first grating we pulled the fiber 16 ± 1 mm with respect to the prism and UV beam before exposing the second grating, thereby producing a non-UV-exposed cavity 12.5 ± 1 mm long. This corresponds to a cavity free spectral range ($\text{FSR} = c/2nL$, where c is the speed of light, n in the index of refraction, and L is the cavity length) of approximately 7 GHz. It is critical that the second grating's Bragg wavelength match that of the first for lasing to occur. Thus the fiber was pulled carefully to a new position, while we took care not to touch the prism, which could result in a Bragg wavelength offset. Even with these precautions, the Bragg wavelength reproducibility was only approximately ± 0.05 nm. The cavity was surrounded by amplifying sections of fiber—approximately 2 cm before the first grating and 6 cm after the second.

During the writing of the second grating, the Er-doped fiber was pumped with 980-nm light, and the output near 1530 nm was simultaneously monitored. A typical curve is shown in Fig. 2. Initially, no lasing occurred since the second grating was not strong enough and did not match the first grating in wavelength. The laser reached threshold after approximately 200 s, and the lasing power increased rapidly. When the exposure time of the second grating approached that of the first, a maximum was reached. The output power often decreased in a more compli-

cated way, exhibiting a step-like structure, as shown in the figure. This may be due to lasing on side-lobe structures of the grating's spectral profile. After approximately 1200 s, the laser power decreased rapidly. This evolution can be understood in qualitative terms when the evolution of the second grating is considered. The rise and stagnation correspond to this grating, first approaching and then matching the first grating in wavelength. The final decline corresponds to the second grating's reflectance becoming weaker. Use of the Fabry-Perot interferometer at different times during this evolution showed that the laser usually operated in a single-longitudinal, single-polarization mode. A second polarization state would manifest itself as an easily detectable second wavelength that is due to the small, natural birefringence of the fiber. Sometimes, however, the laser became multimode with one additional longitudinal mode and/or an orthogonal polarization mode coming above threshold. This happened particularly near the time of maximum power output and can become a serious problem when single-mode, maximum power operation is sought. We tried to solve this problem by postprocessing the cavity with UV radiation, thus slightly changing the phase between the gratings and in this way moving one of the two modes below threshold. Using a 3-mm-long UV beam for postprocessing, we observed the lasing modes to move down in frequency and exchange power, but single-mode operation could not be achieved. This may indicate that postprocessing requires narrower bandwidth gratings or higher index change.

Four fiber lasers were fabricated for further investigation in which the second UV exposure was stopped at points indicated by the four downward pointing arrows in Fig. 2. The illustrated curve is merely a typical example; actual times and peak values varied due to variations of alignment and UV power. These four fiber lasers have different grating overlaps and different strengths of the second grating relative to the first. All operated in a single longitudinal-polarization mode, except the third, which exhibited two longitudinal modes.

4. Laser versus Pump Power Characterization

The output power was measured from both sides of the fiber laser as a function of pump power coupled into the Er-doped fiber. Corrections for transmission loss through the remaining fiber system and gain in the extra Er-doped fiber were made to obtain the total, unamplified laser output. The values for the 980-nm pump power given here are the powers that were coupled into the Er fiber, not the power emitted from the pump laser. The curves of laser power versus pump power were nearly linear with thresholds between 0.9 and 5 mW and slopes ranging from 3 to 4 $\mu\text{W}/\text{mW}$, as shown in Table 1. The maximum power coupled into the Er-doped fiber was approximately 140 mW, which resulted in approximately 0.5 mW of total, unamplified laser output. Despite the differences in the laser cavity characteristics, we did

Table 1. Slope and Threshold of Fiber Laser versus Pump Power Curves^a

Fiber Laser No.	Slope ($\mu\text{W}/\text{mW}$)	Threshold (mW)
1	2.9	3
2	3.7	1.5
3	3.8	5
4	3.9	0.9

^aHere, and in the remaining text, the fiber lasers are referred to as nos. 1, 2, 3, and 4, ordered by increased exposure time for grating 2.

not observe dramatic variations in slopes and thresholds among the four lasers.

5. Output Degeneration

Under initial tests, all the fabricated fiber lasers retained their mode structure within the entire range of applicable pump powers, i.e., single-mode operation did not degenerate into dual-mode operation for higher pump powers and vice versa. Furthermore, the laser output wavelength remained constant within a few hundredths of a nanometer over a period of 2–3 weeks after fabrication. This small variation can be accounted for by room-temperature changes of a few degrees Celsius; the thermo-optic coefficient and thermal expansion of the fiber cause the wavelength of a grating to shift approximately 0.01 nm/ $^{\circ}\text{C}$.

However, after a few hours of continuous pumping, we noticed a downward shift of the laser wavelength. The wavelength shifts always occurred in multiples of approximately 7 GHz, which corresponds to the cavity FSR. For the fiber lasers with gratings that differed the most (i.e., nos. 1 and 4), this mode hopping to shorter wavelengths was accompanied by the appearance of a second longitudinal mode in the laser output, as shown in Fig. 3. Over the course of a few hours, this second mode grew stronger and eventually reached a steady state at an intensity similar to the first. The second mode always appeared at one

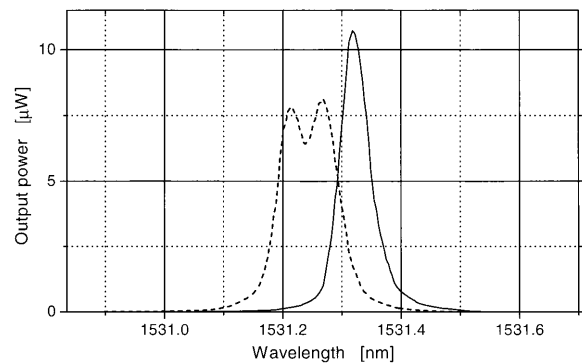


Fig. 3. Degeneration of fiber laser output associated with optical pumping at 980 nm as observed with the OSA (resolution 0.05 nm). The solid and dashed curves represent the output before and after degeneration occurred, respectively.

FSR shorter wavelength with respect to the original mode.

This wavelength shift was irreversible and was not affected by temperature changes to $\pm 10^\circ\text{C}$. One possibility is that the degeneration was caused by thermal bleaching of the gratings due to heating of the Er-doped fiber core by the pump power. To measure the heating caused by the pump laser, we varied the pump power and measured the shift of the laser frequency. We observed a shift of only 400 MHz when varying the pump power from 15 to 80 mW. Assuming that this change is due purely to thermally induced effects, we can place an upper limit on the pump-induced heating of 0.3°C . Thus the pump-induced heating effects are small and cannot explain the laser output degeneration.

The fact that this behavior occurred after several hours of continuous optical pumping leads us to conclude that some optical effect associated with the presence of high-intensity 980-nm radiation (approximately 10^5 W/cm^2) in the fiber core is responsible. It is possible that the 980-nm radiation is optically bleaching the UV-induced refractive-index change or changing the average index of refraction in the fiber core. This would cause a shift of the Bragg wavelength of the fiber gratings. Another more speculative possibility is that the Er gain properties are being modified by the 980-nm light. UV-induced reduction of the lifetime of the upper lasing level in Er-doped waveguides has been observed recently⁸; we may be observing a related effect. However, the physical cause of this process and whether 980-nm radiation can contribute to it are not yet clear.

6. Laser Intensity and Frequency Noise

One of the advantages of fiber lasers that incorporates UV-induced Bragg gratings is that these devices are integrated in the fiber core, thus eliminating use of bulk components. Such devices should yield a more stable output since noise associated with mechanical vibrations of individual bulk components is absent. We characterized the intensity and frequency noise spectra of Bragg-grating Er fiber lasers and compared these with similar measurements made on 1.5- μm lasers incorporating bulk elements. No precautions were made to stabilize the vibrational, acoustic, or thermal environment of the lasers since we were interested in examining the stability against external perturbations. For the comparison of integrated fiber lasers with a bulk component laser we used a single-mode helium–neon laser operating at 1523 nm. This laser has a heavy frame of Invar rods for increased stability. In another study,³ the helium–neon laser's frequency noise was found to be comparable to an Er-doped fiber laser that contained bulk elements.

Relative intensity noise (RIN) was measured with an InGaAs detector, an amplifier, and a 0–100-kHz dynamic signal analyzer. To be sure that no residual pump power contributed to the measurement, a 0.5-mm-thick silicon plate was placed in front of the detector. For a multimode source this setup yields

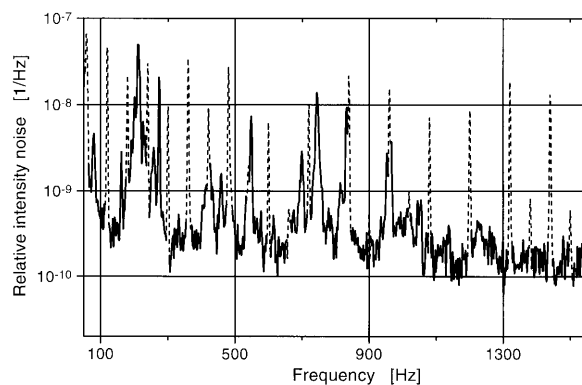


Fig. 4. Relative intensity noise of the dual-mode fiber laser (no. 3). The narrow peaks highlighted by a dashed curve occur at multiples of 60 Hz and are associated with electronic pickup in the detection system.

the RIN of the total output power. The RIN of individual modes can be measured when the Fabry–Perot interferometer's transmission band is centered on the laser line and a single mode for characterization is selected.

The frequency response of the detection setup was investigated by use of a LiNbO_3 modulator after the fiber laser to produce a variable frequency and constant amplitude modulation. The detected, normalized modulation amplitude was equal to 1 for frequencies to 20 kHz, after which it decreased exponentially, reaching 0.07 at 100 kHz. All measurements were normalized to this frequency response curve. Without light reaching the detector, a dark current noise spectrum was obtained and subtracted from subsequent measurements. The detection electronics were sensitive to electrical pickup, and thus both dark current and laser intensity noise exhibited narrow peaks at multiples of 60 Hz. We tried to minimize the effect, but were unable to completely eliminate these peaks. A typical example showing the 60-Hz peaks is illustrated in Fig. 4. At various times the pickup could be several orders of magnitude larger or smaller than shown in Fig. 4, thus prohibiting us from obtaining reliable noise data around these frequencies. To avoid confusion with other resonant features that did not vary significantly over time, we manually removed peaks occurring at multiples of 60 Hz in the following graphs.

Figure 5 illustrates the mean-square RIN of the bulk-component helium–neon laser and fiber lasers no. 2 (single mode) and no. 3 (dual mode) operating with 70 mW of pump power. Each curve consists of two measurements normalized to the measurement bandwidth: one low-frequency (0–1.56-kHz) narrow bandwidth (2.93-Hz) spectrum and another high-frequency (1.56–100-kHz) broad bandwidth (187-Hz) spectrum. The bulk laser has a broad RIN spectrum without resonant features, peaking at a magnitude of approximately $7 \times 10^{-8}\text{ Hz}^{-1}$ at a few kilohertz. The single-mode fiber laser exhibits much less noise, with low-frequency resonant features around a few hundred hertz, peaking at approximately 6×10^{-10}

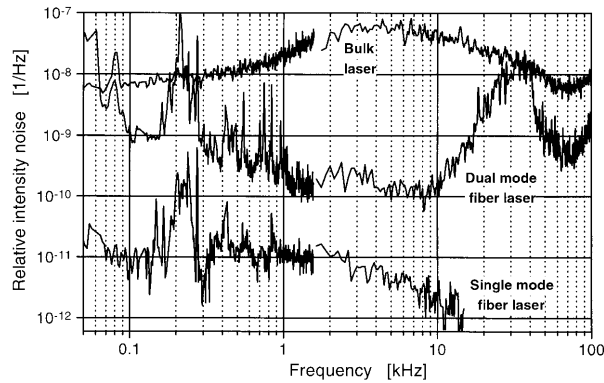


Fig. 5. RIN spectra of the bulk helium–neon laser, a dual-mode fiber laser (no. 3), and a single-mode fiber laser (no. 2). The plotted curve for the dual-mode laser illustrates the RIN of a single mode and not the total power. Peaks occurring at multiples of 60 Hz have been filtered from the low-frequency data.

Hz^{-1} . The curve shown in Fig. 5 does not extend beyond 15 kHz since the dark current noise background exceeded the laser RIN in this range. The overall intensity noise of the single-mode fiber laser is 3–4 orders of magnitude less than that of the bulk laser. In fact, this noise spectrum is identical to the RIN spectrum of the pump laser; that is, no excess RIN noise is introduced by the fiber laser in this frequency range.

The multimode fiber lasers exhibited spectra with similar resonant features, but the total RIN was approximately 15 times larger than that of the pump laser. Selection of a single mode for analysis (Fig. 5) resulted in a RIN signal peaking at 10^{-7} Hz^{-1} , which is even larger than the peak value of the bulk laser and 2 orders of magnitude larger than that of the single-mode fiber laser. The overall RIN observed in dual-mode operation was approximately 20–100 times larger than that obtained for single-mode operation, clearly illustrating the effects of mode competition. The broad peak around 40 kHz is due to relaxation oscillations. When we lowered the pump power, relaxation oscillations could also be observed for the single-mode fiber laser, as discussed in the following section.

We measured frequency noise by placing the Fabry–Perot interferometer in front of the InGaAs detector while weakly locking the side of the transmission peak to the free-running laser. In this configuration, a 100-kHz change of laser frequency resulted in a 2.5% change in transmitted power. Frequency jitter at frequencies as low as approximately 50 Hz could be measured without being affected significantly by the locking electronics. An upper limit of 100 kHz was given by the dynamic signal analyzer. This range includes low-frequency noise (typically below 10^4 Hz), which is usually not sampled by experiments with self-heterodyne delay techniques.

The method of using a weakly locked Fabry–Perot resonator for frequency noise measurements involves two complications: (1) lack of discrimination be-

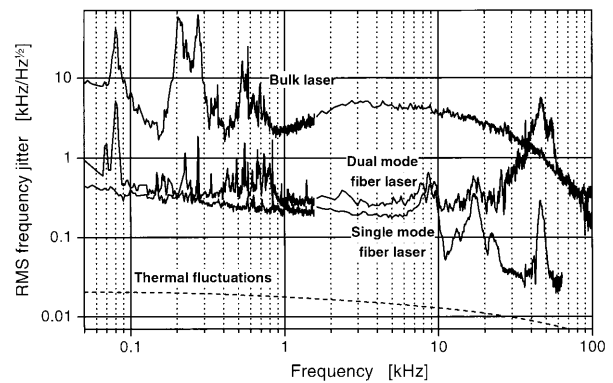


Fig. 6. Frequency noise spectra of the bulk helium–neon laser, a dual-mode fiber laser (no. 3), and the single-mode fiber laser (no. 2). The dashed curve represents the fundamental limit that is due to thermal fluctuations of the fiber laser cavity. Peaks occurring at multiples of 60 Hz were filtered from the low-frequency data.

tween intensity and frequency noise, and (2) lack of discrimination between variations of laser frequency and Fabry–Perot mirror separation. The former was not an issue because the intensity noise component for all lasers was more than 1 order of magnitude smaller than the frequency noise component. The latter is more difficult to address, since we do not have an ideally stable source to check the Fabry–Perot. However, we noticed that the observed low-frequency noise spectrum from the fiber lasers was sensitive to how the laser was mounted. Below 1 kHz, the spectrum contained resonance peaks as high as 100 times stronger when the fiber laser was placed inside a large book, than when it was lying freely on the optical table. This suggests that a considerable fraction of the observed noise is due to the fiber laser and not the Fabry–Perot. However, the frequency noise data for the most stable fiber lasers should be regarded as an upper limit for the actual noise. For the lasers that were less stable, the Fabry–Perot noise contribution is negligible.

Figure 6 illustrates the rms frequency noise spectra of the helium–neon laser and the same fiber lasers used in Fig. 5 (70-mW pump power). The plotted frequency jitter is the result after we subtracted the intensity noise spectra and performed the previously mentioned corrections for dark current background and measurement bandwidth. The bulk laser exhibits large rms frequency jitter approaching $100 \text{ kHz/Hz}^{1/2}$ at various frequencies below 1 kHz. Beyond a few kilohertz no resonant features appear and the noise drops steadily, reaching approximately $0.1 \text{ kHz/Hz}^{1/2}$ at 100 kHz. This behavior is consistent with the results of a previous study involving the same laser.³ That study showed that this helium–neon laser exhibited frequency jitter similar in magnitude to that of a linear single-longitudinal-mode Er fiber laser incorporating coupled cavities and a bulk diffraction grating. In our current study, the frequency noise of the single-mode fiber laser incorporating fiber gratings proves to be substantially less than the bulk laser, with frequency deviations on

average 20 times smaller. The spectrum contains a few narrow resonance peaks below 1 kHz and three broader features between 8 and 45 kHz. None of these exceed 0.6 kHz/Hz^{1/2} in magnitude, which is approximately 100 times smaller than corresponding features seen with bulk lasers.

Figure 6 also shows the frequency noise spectrum of one mode of a dual-mode laser. The background frequency noise for the dual-mode fiber laser is similar to that of the single-mode laser. However, dual-mode operation results in many narrow resonances peaking at several kilohertz per root hertz at frequencies below 1 kHz. The broad feature around 40 kHz is due to the relaxation oscillations that are also visible as intensity noise in Fig. 5.

The fiber laser frequency noise is limited fundamentally by temperature fluctuations within the laser cavity, giving rise to small variations of length and refractive index. In this limit the frequency noise spectrum is given by

$$\Delta\nu(\omega) = \frac{c}{2\pi nL} \sqrt{4\pi S_{\phi\phi}(L, \omega)}, \quad (1)$$

where $S_{\phi\phi}(L, \omega)$ is the spectral function governing the thermal phase noise.⁹ The dashed curve in Fig. 6 illustrates the frequency jitter that is due to thermal fluctuations of the fiber laser cavity, calculated with results from Ref. 9. This calculation shows that the frequency noise of the single-mode fiber laser is approximately 1 order of magnitude above the thermal limit.

We can obtain the total frequency noise over a measurement range by taking the square root of the integrated mean-square frequency noise. For the measurement range in Fig. 6 (50 Hz–63 kHz), we obtain an integrated rms frequency noise of 36 kHz for the single-mode fiber laser. Although this is 13 times larger than the thermal limit, it is remarkably low for an unstabilized laser. In comparison, the integrated rms frequency noise of the dual-mode fiber laser is 450 kHz and that of the helium–neon laser is 720 kHz (50-Hz–100-kHz range).

7. Relaxation Oscillations

The fiber laser power exhibited relaxation oscillations having peak-to-peak amplitudes ranging from a few parts per million to 1% of the average power. Such amplitudes may seem insignificant; however, as shown in the previous section, relaxation oscillation may give rise to significant frequency fluctuations.

For all fiber lasers the relaxation oscillation frequency and amplitude, as observed in the RIN spectra, were measured as a function of normalized pump power, $r = P_{\text{pump}}/P_{\text{threshold}}$. Representative data for single-mode and dual-mode lasers are shown in Figs. 7 and 8. The spectra are obtained for the total laser power, without use of the Fabry–Perot for selection of individual modes. The pump power was varied so that the relaxation oscillation frequency was sampled throughout most of the measurement range to 100 kHz. As can be seen in Fig. 7, the observed frequen-

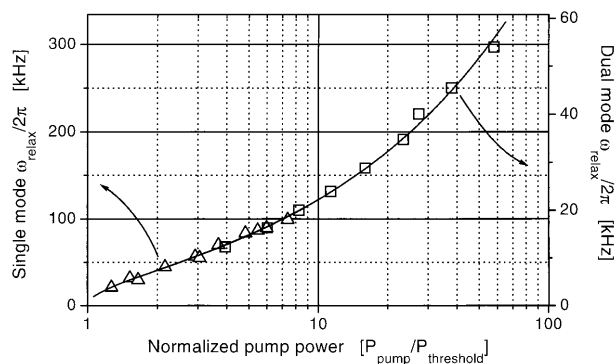


Fig. 7. Relaxation oscillation frequency for a single-mode (triangles) and dual-mode (squares) fiber laser (nos. 2 and 4) as a function of normalized pump power. The solid curve illustrates the theoretical $(r - 1)^{1/2}$ dependence.

cies closely match the theoretically expected $(r - 1)^{1/2}$ dependence. However, for a given pump power the single-mode laser relaxation oscillation frequency is approximately five times higher than its dual-mode counterpart. Because complex behavior can occur in multimode lasers due to mode hopping and mode competition, it is difficult to derive conclusions from this observation. It is also possible that additional oscillation features are present above 100 kHz.

The relaxation oscillation amplitude, as observed in the RIN spectra, versus the normalized pump power is shown in Fig. 8. For the single-mode fiber laser the amplitude decreases from approximately $5 \times 10^{-5} \text{ Hz}^{-1}$ just above threshold to approximately $1 \times 10^{-5} \text{ Hz}^{-1}$ at three times threshold. For higher pump powers the measured amplitude remains constant. The relaxation oscillation amplitude of the dual-mode fiber laser is generally smaller than that of the single-mode fiber laser. Furthermore, it decreases steadily for all pump powers, from approximately 10^{-7} Hz^{-1} near threshold to approximately 10^{-11} Hz^{-1} at the maximum pump power (60 times threshold). The data illustrate, in a qualitative manner, that the multimode fiber laser's relaxation oscillations are more damped than those in the single-mode laser. Multimode operation also in-

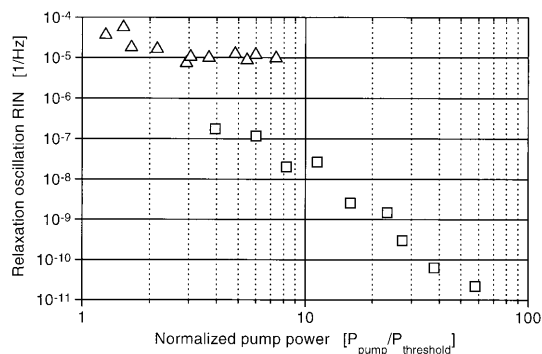


Fig. 8. Relaxation oscillation amplitude for a single-mode (triangles) and dual-mode (squares) fiber laser (nos. 2 and 4) as a function of normalized pump power.

creases the damping of relaxation oscillations in semiconductor lasers by effectively increasing the spontaneous emission factor.¹⁰ The amplitude data for the dual-mode laser should be interpreted with caution since additional noise that is due to mode competition has been excluded by the measurement procedure.

8. Conclusion

Short, Er-doped fiber lasers have been fabricated with two UV-induced Bragg gratings written directly into the doped fiber. We have demonstrated a simple method for real-time monitoring of the laser power and number of oscillating modes by pumping the Er-doped fiber during the UV exposure. This method is useful since these parameters vary considerably over a short time during the UV exposure due to the time-dependent spectral overlap and relative phase shift between the two gratings.

We have observed mode hopping of the fiber laser output, which seems to be optically induced by the pump laser during the first few hours of operation. The effect is irreversible and in some cases includes a degeneration of single-mode operation into dual-mode operation. To our knowledge, such pump-induced output degeneration has not been reported previously and should be taken into account if stable single-mode operation is to be achieved.

Finally, we have shown that single-mode fiber grating lasers have an overall relative intensity noise 3–4 orders of magnitude lower than a single-mode helium–neon laser. In our experiments, this level is limited by noise in the pump laser and may be reduced further by use of a more stable pump source. The frequency stability is also significantly better than the helium–neon laser, with very few mechanical resonances, none of which exceed 0.6-kHz/Hz^{1/2} rms. The total frequency noise, integrated from 50 Hz to 63 kHz, was 36-kHz rms. Without any steps to improve the stability further, we observed the frequency noise spectrum to be only approximately 1 order of magnitude larger than the theoretical limit imposed by thermal fluctuations of the laser cavity. In comparison, bulk lasers typically exhibit frequency

instabilities that are 2 orders of magnitude larger. The fiber laser frequency stability may be degraded by relaxation oscillations that give rise to fluctuations several orders of magnitude above the background level. If lower-frequency noise is required, active intensity noise suppression schemes^{1,2} could be employed to reduce this component.

We thank K. L. Walker and D. J. DiGiovanni (AT&T, Murray Hill) for providing the Er-doped fiber and J. Amin and J. Wells for helpful comments.

References and Note

1. V. Mizrahi, D. J. DiGiovanni, R. M. Atkins, S. G. Grubb, Y.-K. Park, and J.-M. P. Delavaux, "Stable single-mode erbium fiber-grating laser for digital communication," *J. Lightwave Technol.* **11**, 2021–2025 (1993).
2. G. A. Ball, C. E. Holton, G. Hull-Allen, and W. W. Morey, "60 mW 1.5 μm single-frequency low-noise fiber laser MOPA," *IEEE Photon. Technol. Lett.* **6**, 192–194 (1994).
3. S. L. Gilbert, "Frequency stabilization of a tunable erbium-doped fiber laser," *Opt. Lett.* **16**, 150–152 (1991).
4. R. W. Fox, S. L. Gilbert, L. Hollberg, and J. H. Marquardt, "Optical probing of cold trapped atoms," *Opt. Lett.* **18**, 1456–1458 (1993).
5. J. L. Zyskind, V. Mizrahi, D. J. DiGiovanni, and J. W. Sulhoff, "Short single frequency erbium-doped fibre laser," *Electron. Lett.* **28**, 1385–1387 (1992).
6. H. Patrick and S. L. Gilbert, "Growth of Bragg gratings produced by continuous-wave ultraviolet light in optical fiber," *Opt. Lett.* **18**, 1484–1486 (1993).
7. The fiber used was AT&T DID920612-1. We use company and trade names to specify the experimental procedure adequately and do not imply endorsement by the National Institute of Standards and Technology.
8. J. Hübner, T. Feuchter, C. V. Poulsen, and M. Kristensen, "Directly UV-written erbium doped waveguides," in *Photosensitivity and Quadratic Nonlinearity in Glass Waveguides: Fundamentals and Applications*, Vol. 22 of 1995 OSA Technical Digest Series (Optical Society of America, Washington, D.C., 1995).
9. K. H. Wanser, "Fundamental phase noise limit in optical fibres due to temperature fluctuations," *Electron. Lett.* **28**, 53–54 (1992).
10. Y. Suematsu and A. Adams, eds., *Handbook of Semiconductor Lasers and Photonic Integrated Circuits* (Chapman and Hall, London, 1994), p. 273.